JOURNAL OF MOLECULAR SPECTROSCOPY **101**, 104–132 (1983)

Calculation of the Rotation–Vibration Spectrum of NH^+

LESLIE FARNELL AND JOHN F. OGILVIE[1]

Research School of Chemistry, Australian National University, Canberra, A.C.T. 2601, Australia

Ab initio molecular orbital calculations have been used to compute potential energy and dipole moment functions for the $X^2\Pi$ and $a^4\Sigma^-$ states of NH^+. These functions have been used to compute rotational–vibrational energy levels, including the interaction between the two states. Transition moments have been calculated for transitions between these levels, using either the results of numerical diagonalization of the Hamiltonian, or more approximately by fitting analytic functions. Good agreement with experimental data is found, and our results have also been used to interpret previously unassigned spectral lines.

INTRODUCTION

The NH^+ ion is of interest as an example of a diatomic species with a $^2\Pi$ ground state. This is one of the more common types of nondegenerate ground state. Unlike other molecules in this class such as the isoelectronic molecule CH, NH^+ has not been intensively studied. The main experimental investigations of the ground state have been those of Feast (*1*) and Krishnamurthy and Saraswathy (*2*), who studied the $C^2\Sigma^+$–$X^2\Pi$ system, and of Colin and Douglas (*3*), who studied the $A^2\Sigma^-$–$X^2\Pi$ and $B^2\Delta$–$X^2\Pi$ systems. These workers found that the $^2\Pi$ state is severely perturbed by a $^4\Sigma^-$ state, which causes the observed spectrum to be complicated; indeed many of the observed spectral lines remain unassigned. The $a^4\Sigma^-$–$X^2\Pi$ interaction has been studied theoretically by Wilson (*4*), with the aim of predicting Λ-type doubling frequencies of NH^+ and isotopically substituted species. In other work (*5–7*) only potential energy curves have been calculated, without consideration of the fine structure.

In the present work we have reexamined the $^4\Sigma^-$–$^2\Pi$ interaction. We are able to suggest assignments for most of the previously unassigned lines. As well as potential energy curves, dipole moment functions have been calculated. Thus we have been able to investigate the relative intensities of the various transitions. We have done this in two ways, either by a proper diagonalization of the Hamiltonian matrix, or else by an approximate technique based on analytic functions.

DESCRIPTION OF CALCULATIONS

Potential energy and dipole moment functions were calculated for the $a^4\Sigma^-$ and $X^2\Pi$ states of NH^+. The limits for the united atom and dissociation products of these states are shown in Fig. 1. The $a^4\Sigma^-$ state is well described by the single electronic

[1] Address from 1983: Department of Chemistry, Bahrain University College, P.O. Box 1082, Manama, Bahrain.

0022-2852/83 $3.00

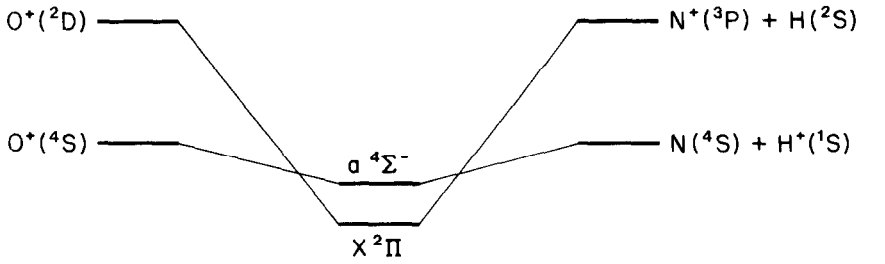

FIG. 1. Limits for the united atom and dissociation products of the $X^2\Pi$ and $a^4\Sigma^-$ states of NH^+.

configuration $1\sigma^2 2\sigma^2 3\sigma 1\pi^2$ for all internuclear separations. However, the $X^2\Pi$ state requires the following three configurations for dissociation to be properly described:

$$1\sigma^2 2\sigma^2 3\sigma^2 1\pi$$

$$1\sigma^2 2\sigma^2 4\sigma^2 1\pi$$

$$1\sigma^2 2\sigma^2 (3\sigma 4\sigma)^T 1\pi.$$

Here the superscript T indicates triplet coupling of the 3σ, 4σ pair. Ab initio molecular orbital calculations using only these configurations were carried out using a modified version of the ALIS suite of computer programs (*8*). Near the potential energy minimum the $X^2\Pi$ wavefunction is dominated by the first of the given configurations. Therefore calculations are also reported for this region which use this configuration alone. All of these few-configuration wavefunctions will be called "SCF" hereafter.

Because the NH^+ molecule has a net charge, the value of the dipole moment depends on the coordinate system chosen. The numbers reported correspond to siting the origin at the center of mass, with the hydrogen atom lying in the positive direction.

The SCF wavefunctions proved to be inadequate for computing the potential energy curves, especially for the $a^4\Sigma^-$ state. Therefore further calculations were carried out incorporating the effects of electron correlation by means of a Møller-Plesset perturbation expansion (*9, 10*) truncated at third order. These calculations will be denoted UMP3, the U signifying that an unrestricted Hartree–Fock wavefunction (*11*) is used as a starting point for the expansion. The UMP3 calculations were carried out using a modified version (*12*) of the Gaussian 80 system of programs (*13*).

In all of the calculations, the same basis set was employed, following previous work (*14*). For hydrogen the 6*s* set of Huzinaga (*15, 16*) was used, augmented by two sets of *p* functions with exponents 1.0 and 0.25. For nitrogen the 11*s*6*p* set of van Duijneveldt (*17*) was used, augmented at the diffuse end by adding an *s* function (exponent 0.055) and a set of *p* functions (exponent 0.05). In addition two sets of *d* polarization functions with exponents 0.25 and 1.0 were placed on the nitrogen nucleus. The primitive basis set was contracted as previously described (*14*).

One further computer program was used in this work. This is the CDIST program of Hutson (*18, 19*), used to calculate vibrational wavenumbers from the potential energy function by numerical solution of the one-dimensional Schrödinger equation. This program was modified to carry out vibrational averaging of various quantities such as spin–orbit coupling constants.

RESULTS

(a) Potential Energy and Dipole Moment Functions

The potential energy functions are presented in Tables I and II and Fig. 2. Dipole moment functions are presented in Table III and Fig. 3. The latter merit further discussion because of the dependence on coordinate system. The dipole moment can be usefully expressed as the sum of two terms,

$$M = M_{PC} + M_B$$

Here M_{PC} is the dipole moment that would be found if a point charge were placed on the appropriate atom, as determined by the dissociation limit. The total M asymp-

TABLE I

Calculated Total and Relative Energies for the $X^2\Pi$ State of NH^+

Internuclear distance /10^{-10} m	1 configuration /hartree	3 configurations /hartree	UMP3 /hartree	3 configurations /cm^{-1}	UMP3 /cm^{-1}
0.7	-54.311648	-54.323325	-54.428583	13856.5	9896.4
0.8	-54.430329	-54.444477	-54.549129	-12733.3	-16560.4
0.9	-54.485090	-54.502011	-54.605935	-25360.5	-29027.8
0.950			-54.620006		-32116.2
1.000	-54.504706	-54.524708	-54.627732	-30341.9	-33811.8
1.060			-54.630931		-34513.9
1.070			-54.630963		-34520.9
1.077			-54.630914		-34510.0
1.085			-54.630788		-34482.4
1.095			-54.630533		-34426.4
1.100	-54.505032	-54.528421		-31156.8	
1.150			-54.627454		-33750.7
1.2	-54.494989	-54.522035	-54.622736	-29755.3	-32715.3
1.3	-54.479667	-54.510620	-54.609833	-27250.0	-29883.4
1.4			-54.594170		-26445.8
1.5	-54.443751	-54.483032	-54.575649	-21195.1	-22380.8
1.6			-54.554584		-17757.6
1.7	-54.408922	-54.456814	-54.536316	-15440.9	-13748.2
1.8			-54.522403		-10694.7
2.0	-54.365653	-54.426318	-54.504117	-8747.8	-6681.4
2.2	-54.343278	-54.412317	-54.493302	-5675.0	-4307.8
2.5	-54.318036	-54.399365	-54.484123	-2832.3	-2293.3
3.0	-54.292151	-54.390598	-54.477484	-908.2	-836.2
3.5	-54.278707	-54.387973	-54.475182	-332.1	-331.0
4.0	-54.271895	-54.387138	-54.474373	-148.8	-153.4
4.5			-54.474054		-83.3
5.0	(a)	-54.386678	-54.473901	-47.8	-49.8
7.0	(a)	-54.386510	-54.473725	-11.0	-11.2
10.0	(a)	-54.386472	-54.473686	-2.6	-2.7
15.0	(a)	-54.386462	(a)	-0.4	
20.0	(a)	-54.386461	(a)	-0.2	
∞		-54.386460	-54.473674	0.	0.

(a) Convergence problems observed.

TABLE II

Calculated Total and Relative Energies for the $a^4\Sigma^-$ State of NH^+

Bondlength /10^{-10} m	1 configuration /hartree	UMP3/hartree	1 configuration /hartree	UMP3/cm^{-1}
0.7	-54.349686	-54.434621	10929.8	15378.8
0.8	-54.466353	-54.554029	-14675.6	-10828.2
0.9	-54.520150	-54.610731	-26482.7	-23272.9
0.950		-54.625177		-26443.4
1.000	-54.540015	-54.633563	-30842.5	-28284.1
1.060		-54.637925		-29241.2
1.070		-54.638189		-29299.1
1.077		-54.638307		-29325.2
1.085		-54.638380		-29341.2
1.090		-54.638393		-29344.0
1.095		-54.638382		-29341.6
1.100	-54.541853		-31245.9	
1.150		-54.636894		-29015.1
1.2	-54.534561	-54.633863	-29645.5	-28349.9
1.3	-54.523132	-54.624949	-27137.2	-26393.3
1.4		-54.614227		-24040.2
1.5	-54.497685	-54.603104	-21552.2	-21599.0
1.6		-54.592318		-19231.6
1.7	-54.475117	-54.582222	-16599.1	-17015.9
1.8		-54.572945		-14979.9
2.0	-54.448977	-54.556830	-10862.0	-11443.0
2.2	-54.435514	-54.543678	-7907.2	-8556.5
2.5	-54.420030	-54.528916	-4508.9	-5316.6
3.0	-54.406343	-54.513056	-1504.9	-1835.6
3.5	-54.402060	-54.507557	-564.9	-628.8
4.0	-54.400721	-54.505956	-271.1	-277.4
5.0	-54.399935	-54.505125	-98.5	-95.1
7.0	-54.399599	-54.504800	-24.8	-23.8
10.0	-54.399513	-54.504718	-5.9	-5.6
15.0	-54.399491	(a)	-1.1	-
20.0	-54.399488	-54.504693	-0.4	-0.3
∞	-54.399486	-54.504692	0.	0.

(a) Convergence problems observed.

totically approaches M_{PC} at large internuclear separation. It is given, in our chosen coordinate system, by

$$M_{PC}(X^2\Pi) = -1.07570\ R \times 10^{-30}\ \text{C m}$$

$$M_{PC}(a^4\Sigma^-) = 14.9462\ R \times 10^{-30}\ \text{C m}$$

where R is the internuclear separation in units of 10^{-10} m. The second term M_B is invariant to change of origin. It represents the redistribution of electron density due

TABLE III

Calculated Dipole Moments[a] for NH^+ (10^{-30} C m)

Internuclear distance /10^{-10} m	$X^2\Pi$ 1 configuration	$X^2\Pi$ 3 configurations	$a^4\Sigma^-$ 1 configuration
0.7	5.5232	5.4628	1.4730
0.8	5.8611	5.7617	2.2732
0.9	6.2553	6.0929	3.1146
1.0	6.7206	6.4551	4.3287
1.1	7.2700	6.8461	5.5832
1.2	7.9148	7.2337	6.9585
1.3	8.6637	7.6119	8.4252
1.5	10.498	8.2003	11.435
1.7	12.747	8.3845	14.234
2.0	16.859	7.3761	17.805
2.2	19.976	5.6819	20.477
2.5	25.019	2.7602	26.578
3.0	33.865	-0.8439	40.122
3.5	42.677	-2.6618	50.303
4.0	51.075	-3.6425	58.600
5.0		-5.0478	74.053
7.0		-7.3308	104.277
10.0		-10.682	149.292
15.0		-16.102	224.124
20.0		-21.496	298.881

a. With origin at the centre of mass and H on the positive axis.

to bond formation. Since it arises at large separations from induction of a dipole in the neutral atom by the ion, it vanishes as R^{-2}; this behavior is illustrated in the log–log graph.

The data in Tables I–III may be used to predict term-value coefficients and transition moments that lead in turn to wavenumbers and matrix elements for intensities of vibration–rotational transitions within each electronic state. To use the numerical data it has to be converted into an analytical form, by means of fits to appropriate equations with parameters determined according to standard statistical procedures. In this case the potential-energy data were fitted to members of the following flexible family of truncated polynomials (*20*):

$$V(R) = d_0^{mn} w_{mn}^2 (1 + \sum_{j=1}^{p} d_j^{mn} w_{mn}^j)$$

in which the separation variable

$$w_{mn} \equiv (m + n)(R - R_e)/(mR + nR_e)$$

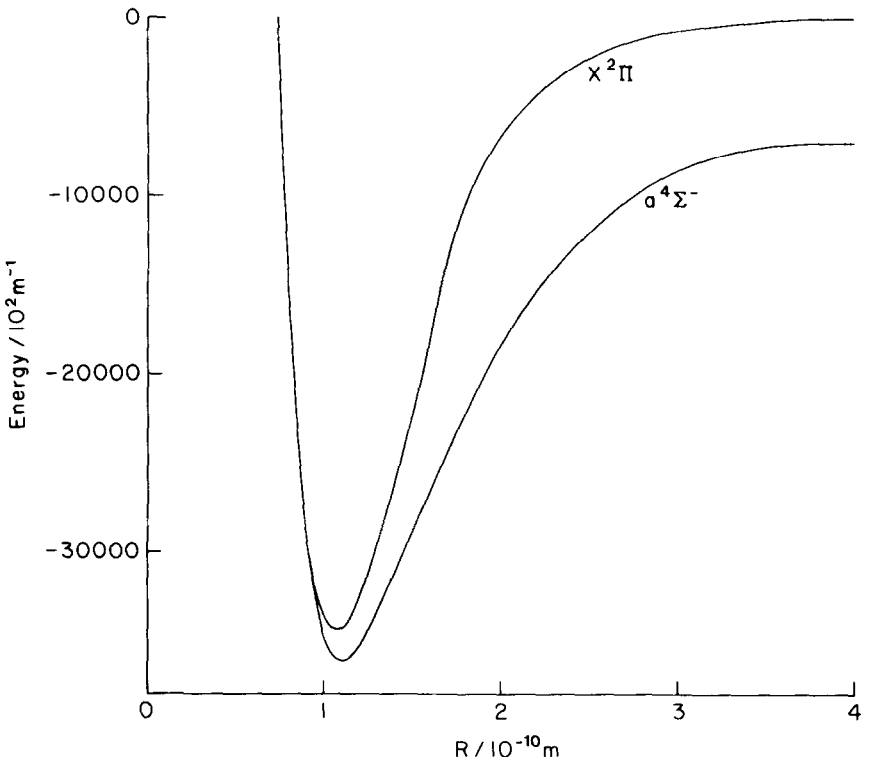

FIG. 2. Potential energy curves for NH^+ calculated at the UMP3 level. The energies are relative to the dissociation limit of the $X^2\Pi$ state.

(containing the integer parameters m and n and the equilibrium internuclear separation R_e) and the coefficients d_j^{mn}, $(0 \leqq j \leqq p)$ were selected to produce the best fit. For the $X^2\Pi$ and $a^4\Sigma^-$ states the parameters $m = n = 1$ and $p = 8$ gave the most satisfactory results. In this case we have, in the notation of Ref. (*20*), $w_{1,1} \equiv z \equiv 2(R - R_e)/(R + R_e)$ and $d_j^{1,1} \equiv c_j$. The values of the coefficient c_j are given in Table IV, together with the values of R_e and $\mathcal{D}_e \equiv V(\infty) - V(R_e)$. For any particular isotopic molecule $c_0 = B_e\gamma^{-2}$, where B_e is the usual equilibrium rotational parameter $h/8\pi^2 c\mu R_e^2$. The value of $\gamma = 2B_e/\omega_e$, where ω_e is the usual vibration frequency, is also given in Table IV.

The appropriate form for the dipole moment function $M_B(R)$ is (*21*)

$$M_B(R) = M_0(x + 1)/(1 + \sum_{j=1}^{3} e_j x^j)$$

where $x = (R - R_e)/R_e$, according to the limiting behavior $M_B(R) \propto R^{-2}$ as $R \rightarrow \infty$. However, the above functional form contains too few adjustable parameters (e_j) to represent the entire set of data accurately. Furthermore the intensities of transitions depend on the full dipole moment M, rather than M_B. Therefore a polynomial fit of the form

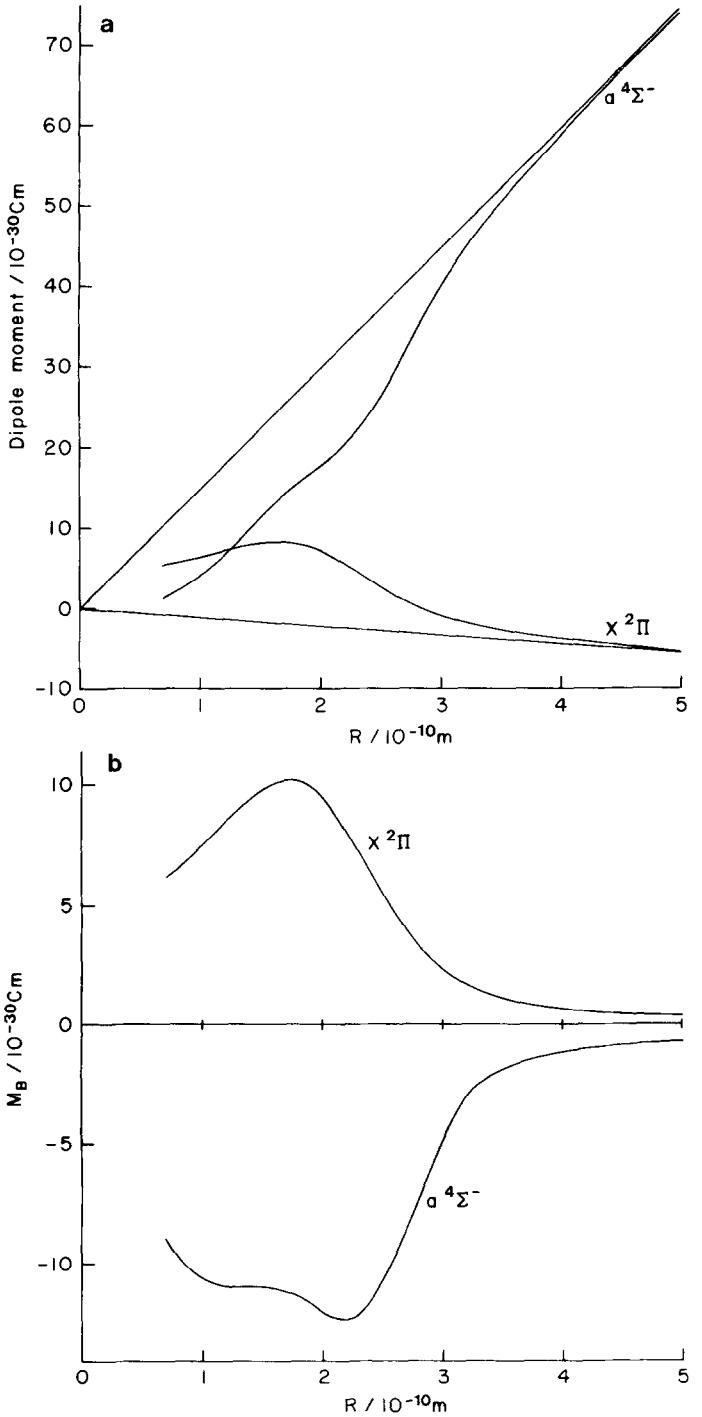

FIG. 3. Dipole moment functions for NH^+ calculated at the SCF level: (a) total dipole moment M and point charge moment M_{PC}; (b) difference $M_B = M - M_{PC}$; (c) long-range behavior, showing slope -2.

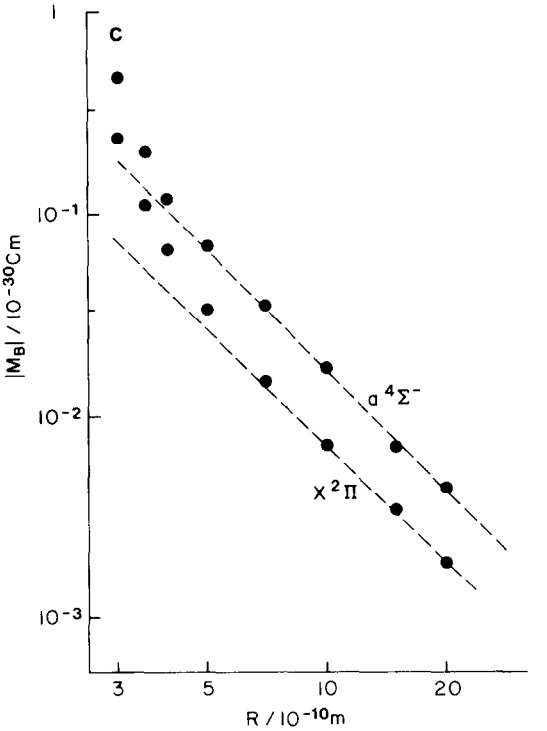

FIG. 3—*Continued.*

$$M(R) = \sum_{j=0}^{k} M_j x^j$$

was made to the data in the region of interest around the equilibrium internuclear separation, specifically $0.7 \leqq R/10^{-10}$ m $\leqq 3.0$. The resulting coefficients are also presented in Table IV.

(b) Vibrational Structure

The energies of the vibrational states calculated using the CDIST program are given in Table V. For the purpose of comparison with experiment the values of $\Delta G(1/2)$ are also given. It should be noted that there is some uncertainty in the experimental values because of the complication of the interaction between the states (*2, 3*).

In the alternative approach we treated the data through the analytic functions described above. The theory has been developed strictly for diatomic molecules in $^1\Sigma$ states, i.e. states without net orbital or spin angular momentum. However, in computing the potential energy and dipole moment data the small terms in the Hamiltonian directly dependent on such properties are omitted. Therefore no inconsistency arises. The additional effects due to angular momenta are considered in the following section.

TABLE IV

Parameters of the Potential Energy and Dipole Moment Functions of NH^+ in Two Electronic States

$X^2\Pi$			$a^4\Sigma$	
c_j	$M_j/10^{-30}$ C m	j	c_j	$M_j/10^{-30}$ C. m
149130.97 cm^{-1}	6.71866	0	127427.04 cm^{-1}	5.45043
-1.4334	4.18508	1	-1.5140	14.1935
1.5753	0.59901	2	0.7695	7.8617
2.9894	-4.30524	3	0.3526	-4.4948
-5.5742	-1.28635	4	0.3523	-12.6371
-9.1716	3.84404	5	-2.3420	-3.5443
22.0617	-10.9791	6	2.5432	29.1578
-14.2812	10.3866	7	-1.1202	-19.6238
3.0506	-2.78394	8	0.1804	3.8128
	-0.47947	9		
0.0102693		γ	0.0108814	
1.06776		R $/10^{-10}$m	1.09014	
34521.78		D_e/cm^{-1}	29344.03	

The mass-reduced term-value coefficients U_{kl} are defined according to

$$E(v, N) = \sum_{k=0} \sum_{l=0} U_{kl}\mu^{-(k+2l)/2}(v + \tfrac{1}{2})^k[N(N+1)]^l$$

where v and N are the vibrational and rotational quantum numbers and μ is the reduced mass. They may be determined from the coefficients c_j of Table IV, using the set of relations given previously (*20*). The results are listed in Table VI. Note that $2U_{0,1}U_{1,0}^{-1} \equiv \gamma \equiv 2B_e\omega_e^{-1}$.

From the potential energy dipole moment parameters, the vibrational matrix elements $\langle 0|x^n|v\rangle$, for $0 \leqq v \leqq 6$ and $1 \leqq n \leqq 8$, were calculated according to analytic expressions based on the Dunham theory (*22, 23*). From the combination of these matrix elements and the coefficients in Table IV, one can calculate both the matrix elements for the vibrational transitions and the Herman–Wallis factors (*24*). These are required to describe fully the intensities of both the vibration–rotational bands and the individual lines within each band. The results are listed in Table VII.

(c) Vibration–Rotation Structure

The energies of the rotational states of NH^+, including also spin–orbit coupling effects, were investigated numerically. Because the $X^2\Pi$ and $a^4\Sigma^-$ states are very close

TABLE V

Calculated[a] Energies Expressed as Wavenumbers (cm^{-1}) for Vibrational States of Various Isotopic Species of NH^+

State	v	NH^+ SCF	NH^+ UMP3	ND^+ UMP3	$^{15}NH^+$ UMP3	$^{15}ND^+$ UMP3
$X^2\Pi$	0	1435	1537.9	1126.6	1534.5	1121.9
	1	4284	4509.9	3323.4	4500.1	3309.8
	2	6984	7364.8	5453.0	7349.1	5431.0
$a^4\Sigma^-$	0	1408	1354.1	993.2	1351.1	989.1
	1	4245	3931.9	2909.5	3923.6	2897.7
	2	6898	6349.1	4738.4	6336.1	4719.7
	$\Delta G(\frac{1}{2})$					
$X^2\Pi$	Calc.	2849	2972.0	2196.8	2965.6	2187.9
	Expt.[b]	2922	2922	2143.04	-	-
$a^4\Sigma^-$	Calc.	2837	2577.8	1916.3	2572.5	1908.6
	Expt.[b]	2520	2520	-	-	-

a Relative to the energy at the relevant potential energy minimum.

b Ref. 3.

in energy, it is necessary to take account of the interaction between them. The method for doing this has been described by Wilson (*4*), and requires diagonalization of the Hamiltonian matrix depicted in Table 1 of Ref. (*4*). Matrix elements of the spin–orbit coupling operator are required. Rather than attempt to compute them from our wavefunctions, we simply use the values from Tables 3 and 4 of Ref. (*4*). However, the vibrational averaging was performed using our calculated functions.

In constructing the Hamiltonian matrix three empirical parameters were introduced, because of deficiencies in the potential energy curves which will be discussed below. The parameters are (i) the separation between the minima of the $X^2\Pi$ and $a^4\Sigma^-$ potential energy curves, (ii) a scale factor by which the energies of all vibrational states in the $X^2\Pi$ state were multiplied, and (iii) the analogous scale factor for the $a^4\Sigma^-$ state. They were varied separately for the three isotopic species $^{14}NH^+$, $^{15}NH^+$, and $^{14}ND^+$ to get the best fit to the reported energies (*3*). The results of the fitting are presented in Table VIII. The residual errors are of the order 5 cm^{-1}. Insofar as our method of fitting is more quantitative than that used by Colin and Douglas (*3*), this represents a new interpretation of the spectrum. Therefore we suggest that the spectroscopic constants in Table VIII may be more reliable than those previously reported (*3*). The good agreement of our $\Delta G(\frac{1}{2})$ value for ND^+ with the experimental value, which is well determined because there are fewer perturbations in this species, supports this view. In particular it appears that the previous estimate of the $^4\Sigma^- - ^2\Pi$

TABLE VI

Mass-Reduced Term-Value Coefficients U_{kl} for the $X^2\Pi$ (the lower value in each pair) and $a^4\Sigma^-$ States of NH^+ (Units of U_{kl} are $m^{-1}u^{(k+2l)/2}$)

k/l	0	1	2	3	4	5	6
0	0	1418.52	-0.15791	8.543×10^{-6}	-1.57×10^{-9}	1.7×10^{-13}	-1.7×10^{-17}
	0	1478.61	-0.14660	8.236×10^{-11}	7.60×10^{-11}	6.0×10^{-13}	-5.0×10^{-17}
1	268892.5	-67.978	-3.824×10^{-4}	2.290×10^{-7}	2.05×10^{-10}	-7.8×10^{-15}	1.8×10^{-17}
	296989.1	-63.311	-8.005×10^{-3}	6.067×10^{-6}	-1.09×10^{-10}	-6.9×10^{-13}	-2.6×10^{-16}
2	-8744.7	0.1933	5.80×10^{-4}	6.50×10^{-8}	2.8×10^{-11}	-2.4×10^{-15}	
	-6490.4	6.839	2.19×10^{-3}	-1.81×10^{-6}	-1.1×10^{-9}	-1.6×10^{-14}	
3	124.1	0.123	1.34×10^{-5}	4.6×10^{-10}	-5.8×10^{-12}		
	877.6	-0.291	-1.06×10^{-2}	-2.8×10^{-7}	4.4×10^{-10}		
4	6.06	-5.6×10^{-4}	-3.0×10^{-6}				
	-96.6	-0.16	1.1×10^{-4}				
5	-0.21						
	-1.4						

separation is too high, and should be reduced from ~550 to ~500 cm^{-1}. A similar point has been made previously by Wilson (*4*) who arrived at a value 525 cm^{-1} by fitting only the $J = 11/2$ levels.

The matrix diagonalization also predicts energies of states which have not been observed experimentally. Since most of these are dominated by $^4\Sigma^-$ configurations this is to be expected. However, certain of them have an appreciable $^2\Pi$ component, and allow us to assign many of the unidentified spectral lines. These assignments are listed in Table IX. These numbers have been checked to ensure that trends in the difference between calculated and experimental numbers are constant between the new assignments and previous assignments. For example, there is a completely new series of $^{14}NH^+$ lines assigned as P_2 type (in the notation of Ref. (*3*)) between 18 708.98 and 18 732.25 cm^{-1}. The calculated energies of the lower states are consistently low, with the error increasing as J decreases. The observed intensities of these lines are also in accord with the weights of the $^2\Pi$ components in the calculated wavefunctions.

In certain cases it is not possible to distinguish between a P_2-type transition and a Q_1-type transition to the same lower state because the energies of the upper states (in the $A^2\Sigma^-$ $v = 0$ state) are very close. These instances are noted in Table IX.

TABLE VII

Matrix Elements and Herman–Wallis Factors for the Vibrational Transitions of NH^+ in Two Electronic States

	$X^2\Pi$				$a^4\Sigma$	
$\langle 0\|M(x)\|v\rangle$ /10^{-30}C m	C_0^v	D_0^v	v	$\langle 0\|M(x)\|v\rangle$ /10^{-30}C m	C_0^v	D_0^v
6.719	0	1.3×10^{-4}	0	5.451	0	6.2×10^{-4}
0.298	-6.7×10^{-2}	1.4×10^{-3}	1	1.095	-1.8×10^{-2}	5.7×10^{-4}
-0.322	-4.2×10^{-2}	6.9×10^{-4}	2	-0.0942	2.4×10^{-2}	1.05×10^{-3}
2.33×10^{-3}	-8.7×10^{-2}	4.5×10^{-3}	3	9.06×10^{-3}	8.3×10^{-2}	2.5×10^{-3}
-2.4×10^{-4}	-0.23	4.0×10^{-2}	4	-1.36×10^{-3}	0.15	4.6×10^{-3}
-2.02×10^{-5}			5	2.09×10^{-4}	0.29	2.1×10^{-2}
			6	3.3×10^{-4}	-0.06	-1.7×10^{-3}

The matrix diagonalization provides not only energies of states but also vibrational wavefunctions. These may be used to compute expectation values of the dipole moment operator, and hence transition moments. By this means we can investigate intensities in more detail than is possible with the analytic functions approach outlined above. For example, we can consider $^2\Pi$–$^4\Sigma^-$ transitions and transitions between the various components of the $^2\Pi$ state. The results are presented in Tables X–XII and Figs. 4 and 5. In Table X the column headings give an indication of the dominant electronic configurations in each rotational state. We define the following linear combinations:

$$^2\Pi_s = 2^{-1/2}(^2\Pi_{1/2} + {}^2\Pi_{3/2}) \qquad ^4\Sigma_s^- = 2^{-1/2}(^4\Sigma_{1/2}^- + {}^4\Sigma_{3/2}^-)$$

$$^2\Pi_a = 2^{-1/2}(^2\Pi_{1/2} - {}^2\Pi_{3/2}) \qquad ^4\Sigma_a^- = 2^{-1/2}(^4\Sigma_{1/2}^- - {}^4\Sigma_{3/2}^-)$$

which are more appropriate in some cases, where there is a gradual change with increasing rotational quantum number. This is associated with a changeover in Hund's coupling case. For the sake of simplicity this point is not considered in Tables XI and XII and Figs. 4 and 5. A further point to notice is that our calculated wavenumbers are given. In some instances a more accurate value could have been obtained, using the experimental data (*2, 3*), but this procedure could not be used consistently.

DISCUSSION

Comparison of the calculated energies of the vibrational states with the available experimental data (Table V) indicate that the SCF wavefunctions are inadequate, especially for the $a^4\Sigma^-$ state. This is confirmed by a comparison of other relevant quantities, which is given in Table XIII. It is clear that inclusion of correlation effects much improves matters, but the order of the $X^2\Pi$ and $a^4\Sigma^-$ states remains wrong. It is well known that the calculation of accurate energy differences between states of

TABLE VIII

Results from Fitting Calculated Curves to Experimental Data

	^{14}NH	^{14}ND	^{15}NH
$E(^4\Sigma^-)-E(^2\Pi)$ [(a)]/cm^{-1}	494	504	495
$^2\Pi$ scale factor[(b)]	0.975	0.97	0.975
$^4\Sigma^-$ scale factor[(b)]	0.985	0.992	0.986
v=0 error[(c)]/cm^{-1}	4.75	1.97	4.96
v=1 error[(c)]/cm^{-1}	4.59	3.41	3.16
$^2\Pi$ scaled $\Delta G(\frac{1}{2})$/cm^{-1}	2898	2151	2891
$^4\Sigma^-$ scaled $\Delta G(\frac{1}{2})$/cm^{-1}	2539	1901	2536

(a) empirical parameter

(b) calculated vibration frequencies all multiplied by these empirical parameters.

(c) mean absolute error

different multiplicity is very difficult, as, for example, in the CH_2 molecule (*25, 26*). This problem has been noticed in previous calculations on NH^+ (*4, 7*). As a check on our computations we calculated the corresponding energy difference in the isoelectronic molecule CH, which is better known experimentally. It is found (Table VIII) that the $a^4\Sigma^-$ state is placed too low by a similar amount in both CH and NH^+.

While the UMP3 energies were used in the remainder of this work, a note of caution should be sounded. It proved to be more difficult to achieve a good analytic fit to the $X^2\Pi$ UMP3 energies than for the $a^4\Sigma^-$ UMP3 case or either SCF case. We believe this is due to the use of a UHF wavefunction as a starting point for the MP3 calculation. This wavefunction allows the proper dissociation limit to be reached using only a single configuration, whereas a spin-restricted (RHF) wavefunction requires three configurations. The proper limit is achieved only at the expense of obtaining a wavefunction which is not an eigenfunction of the spin-squared operator. In contrast the $a^4\Sigma^-$ state of UHF wavefunction shows very little spin contamination, since a single spin-restricted configuration dominates at all internuclear separations. We can estimate in which region the UMP3 energies are likely to be reliable by examining the UHF spin expectation value and the three-configuration SCF configuration weights. These are listed in Table XIV, and suggest an upper limit of $R = 1.4 \times 10^{-10}$ m.

TABLE IX

Assignments of Previously Unidentified Spectral Lines of $^{14}NH^+$ and $^{15}NH^+$ (Units are cm^{-1})

	Observed line[a]	Assignment[b]	Experimental energy[c,d]	Calculated energy[d]
$^{14}NH^+$	18761.33 w	unassigned		
	18746.55 m	J=½ R_2	2887.86	2881[e]
	18732.25 w	J=4½	3057.07	3052
	18729.99 m	J=3½ P_2 (or Q_1)	2971.91	2966
	18720.94 m	J=2½	2913.48	2907
	18708.98 s	J=1½	2880.98	2873
	18692.63 s	J=½ R_1 (or Q_2)	2897.21	2891
	18688.58 s	unassigned		
	18679.82 s	J=½ Q_1	2887.86	2881[e]
	18678.19 w	unassigned		
	18625.15 s	J=1½ P_2 (or Q_1)	2964.81	2958
	18563.13 m	J=1½ R_1 (or Q_2)	3071.04	3070
	18520.05 w	J=2½	3180.53	3180
$^{15}NH^+$	18753.76 w	unassigned		
	18753.39 w	J=½ R_2	2882.19	2876[e]
	18734.89 w	J=3½ P_2 (or Q_1)	2966.91	2966
	18726.97 m	J=2½	2908.61	2906
	18717.53 w	unassigned		
	18715.22 s	J=1½ P_2 (or Q_1)	2876.09	2872
	18700.03 s	?J=½ R_2	2935.55	2936[e]
	18695.76 s	J=½ R_1 (or Q_2)	2895.45	2885
	18686.95 s	J=½ Q_1	2882.19	2876[e]
	18634.87 w	unassigned		
	18633.71 s	?J=½ Q_1	2935.42	2936[e]
	18631.79 s	J=1½ P_2 (or Q_1)	2959.52	2956
	18569.70 w	J=1½ R_1 (or Q_2)	3065.64	3069
	18526.79 w	J=2½	3174.68	3179

a Data from Ref. (3).

b Using notation of Ref. (3).

c For $X^2\Pi$ v=1 state calculated assuming our assignments.

d Energies relative to the lowest rotational state of the $X^2\Pi$ v=0 state.

e These six lines form pairs from each of three lower states.

Since the tail of the $v = 1$ vibrational function extends into this region, we might expect that it would be somewhat distorted. Perhaps for this reason the $^2\Pi$ states required a greater degree of scaling in our fit of the experimental data, as shown in Table VIII.

TABLE X

Calculated Energies of Rotational States for NH^+ Expressed in Wavenumbers (cm^{-1})

v	J	e-levels[b]				f levels[b]			
		$^2\Pi_{1/2}$	$^2\Pi_{3/2}$	$^4\Sigma^-_s$	$^4\Sigma^-_a$	$^2\Pi_{1/2}$	$^2\Pi_{3/2}$	$^4\Sigma^-_{3/2}$	$^4\Sigma^-_{1/2}$
0	½	0	-	383.4		0.3	-	-	441.9
	1½	32.9	100.9	358.9	446.9	33.5	100.9	392.0	530.7
	2½	95.2	192.3	388.0	535.8	96.1	192.4	450.7	648.2
	3½	187.7	314.8	447.1	653.4	189.0	314.8	539.0	794.5
	4½	310.4	467.7	536.1	799.8	312.3	467.7	656.7	969.5
	5½	463.1	645.9[a]	659.6[a]	975.0	466.0	650.7	803.7	1172.9
		$^2\Pi_s$	$^2\Pi_a$	$^4\Sigma^-_{1/2}$	$^4\Sigma^-_{3/2}$	$^2\Pi_s$	$^2\Pi_a$	$^4\Sigma^-_s$	$^4\Sigma^-_a$
		$^2\Pi_{1/2}$	$^2\Pi_{3/2}$	$^4\Sigma^-_s$	$^4\Sigma^-_a$	$^2\Pi_{1/2}$	$^2\Pi_{3/2}$	$^4\Sigma^-_{3/2}$	$^4\Sigma^-_{1/2}$
1	½	2880.5[a]	-	2937.6		2890.7	-	-	2983.4
	1½	2941.4[a]	3032.6[a]	2873.4[a]	2958.2[a]	2942.1[a]	3011.2	2893.6[a]	3070.4
	2½	3005.8[a]	3119.0[a]	2907.0[a]	3034.1[a]	3011.2[a]	3091.6	2950.3[a]	3180.3
	3½	3092.5	3234.6[a]	2966.4	3147.5[a]	3103.7[a]	3206.6	3035.2[a]	3318.0
	4½	3209.4	3379.4[a]	3052.3	3289.2[a]	3222.9[a]	3352.8	3148.7[a]	3483.4
	5½	3356.2	3553.5[a]	3165.1	3458.2[a]	3370.1[a]	3529.2	3290.0[a]	3676.0
		$^2\Pi_s$	$^2\Pi_a$	$^4\Sigma^-_{1/2}$	$^4\Sigma^-_{3/2}$	$^2\Pi_s$	$^2\Pi_a$	$^4\Sigma^-_{3/2}$	$^4\Sigma^-_{1/2}$

a Strong $^4\Sigma^-$-$^2\Pi$ mixing.

b The labelling of parity follows J.M. Brown et al., J. Mol. Spectrosc., 55, 500-503 (1975).

TABLE XI

Calculated Transition Energies (cm^{-1}) and Transition Moments (10^{-30} C m) within the Ground Vibrational State of NH^+

Lower state[a]		R BRANCH							
		Energy → $\Pi_{\frac{1}{2}}$	Moment	Energy → $\Pi_{3/2}$	Moment	Energy → $\Sigma_{\frac{1}{2}}$	Moment	Energy → $\Sigma_{3/2}$	Moment
J	$\Pi_{\frac{1}{2}}(e)$								
½	0.0	32.9	6.09	100.9	-2.99	358.9	0.071	446.9	-0.082
1½	32.9	62.3	6.74	159.4	-0.74	355.1	0.165	502.8	-0.028
2½	95.2	92.5	6.77	219.6	-0.39	351.9	0.208	558.2	-0.011
3½	187.7	122.7	6.77	280.0	-0.26	348.4	0.255	612.2	-0.002
4½	310.4	152.8	6.77	335.5	0.36	349.2	0.162	664.6	0.003
5½	463.1	182.4	6.76	337.5	0.49	403.1	-0.067	715.6	0.006
	$\Pi_{\frac{1}{2}}(f)$								
½	0.3	33.2	6.09	100.7	-3.00	530.4	0.040	391.8	-0.018
1½	33.5	62.6	6.74	158.9	-0.74	614.7	0.026	417.3	0.070
2½	96.1	92.9	6.77	218.7	-0.39	698.4	0.019	442.9	0.089
3½	189.0	123.3	6.78	278.7	-0.24	780.5	0.014	467.7	0.100
4½	312.3	153.7	6.79	338.4	-0.17	860.6	0.107	491.4	0.107
5½	466.0	183.9	6.79	397.3	-0.14	938.6	0.112	514.0	0.112
	$\Pi_{3/2}(e)$								
1½	100.9	5.7	0.72	91.4	6.73	287.1	0.15	434.9	0.11
2½	192.3	4.7	0.36	122.4	6.77	254.8	0.19	461.0	0.12
3½	314.8	4.4	0.22	152.9	6.76	221.3	0.41	485.0	0.13
4½	467.7	4.5	0.15	178.3	-5.43	191.9	4.05	507.4	0.13
5½	645.9	0.3	-0.13	154.7	4.36	220.3	-4.67	532.8	-0.07

TABLE XI—*Continued*

	$\Pi_{3/2}(f)$								
$1\frac{1}{2}$	100.9	4.9	0.72	91.4	6.73	547.2	-0.029	349.8	0.19
$2\frac{1}{2}$	192.4	3.4	0.36	122.4	6.77	602.1	-0.036	346.6	0.22
$3\frac{1}{2}$	314.8	2.5	0.21	152.9	6.77	654.7	-0.039	341.9	0.27
$4\frac{1}{2}$	467.7	1.7	0.14	183.0	6.77	705.2	-0.040	336.0	0.36
$5\frac{1}{2}$	650.7	0.8	0.09	212.6	6.76	753.9	-0.040	329.3	0.52
	$\Sigma_{\frac{1}{2}}(e)$								
$\frac{1}{2}$	383.4	350.4	0.0003	282.5	-0.100	24.4	4.31	63.6	-3.89
$1\frac{1}{2}$	358.9	263.7	0.051	166.6	0.005	29.1	5.80	176.8	0.47
$2\frac{1}{2}$	388.0	200.3	0.039	73.2	-0.047	59.1	5.82	265.4	0.21
$3\frac{1}{2}$	447.1	136.7	0.022	20.5	-0.223	88.9	5.83	352.7	0.13
$4\frac{1}{2}$	536.1	73.0	-0.005	109.8	3.34	123.5	4.82	438.9	0.09
$5\frac{1}{2}$	659.6	14.0	0.008	141.1	3.93	206.7	4.93	519.1	0.14
	$\Sigma_{\frac{1}{2}}(f)$								
$\frac{1}{2}$	441.9	408.4	0.049	340.9	-0.105	88.9	5.47	49.8	1.94
$1\frac{1}{2}$	530.7	434.6	0.024	338.3	-0.101	117.5	5.81	80.0	0.35
$2\frac{1}{2}$	648.2	459.2	0.015	333.4	-0.095	146.3	5.82	109.2	0.17
$3\frac{1}{2}$	794.5	482.2	0.010	326.8	0.089	175.0	5.84	137.8	0.09
$4\frac{1}{2}$	969.5	503.4	0.007	318.7	-0.084	203.5	5.85	165.8	0.06
$5\frac{1}{2}$	1172.9	523.0	0.005	309.6	-0.079	231.7	5.87	192.9	0.03

TABLE XI—*Continued*

	$\Sigma_{3/2}(e)$								
$1\frac{1}{2}$	446.9	351.7	0.044	254.6	0.13	58.9	-0.47	88.9	5.81
$2\frac{1}{2}$	535.8	348.1	0.048	221.0	0.12	88.7	-0.19	117.6	5.83
$3\frac{1}{2}$	653.4	343.0	0.048	185.7	0.12	117.3	-0.10	146.5	5.84
$4\frac{1}{2}$	799.8	336.7	0.047	153.9	-0.12	140.3	0.02	175.2	5.86
$5\frac{1}{2}$	975.0	329.4	0.045	174.4	-0.05	108.8	0.10	203.7	5.88
	$\Sigma_{3/2}(f)$								
$1\frac{1}{2}$	392.0	296.0	0.097	199.7	-0.105	256.1	-0.37	58.7	5.81
$2\frac{1}{2}$	450.7	261.3	0.100	135.9	-0.101	343.7	-0.18	88.3	5.83
$3\frac{1}{2}$	539.0	226.7	0.100	71.3	-0.095	430.5	-0.11	117.7	5.84
$4\frac{1}{2}$	656.7	190.7	0.100	6.0	-0.089	516.2	-0.08	147.0	5.86
$5\frac{1}{2}$	803.7	153.8	0.099	59.6	-0.079	600.9	-0.06	176.4	5.88

Q BRANCH

	J	$\Pi_{\frac{1}{2}}(f)$		$\Pi_{3/2}(f)$		$\Sigma_{\frac{1}{2}}(f)$		$\Sigma_{3/2}(f)$	
	$\frac{1}{2}$	0.3	6.76	-		441.9	0.43	-	
	$1\frac{1}{2}$	0.5	6.73	68.0	-0.071	497.8	0.23	359.1	0.54
$\Pi_{\frac{1}{2}}(e)$	$2\frac{1}{2}$	0.9	6.71	97.1	-0.087	553.0	0.14	355.5	0.63
	$3\frac{1}{2}$	1.3	6.70	127.1	-0.100	606.8	0.10	351.3	0.68
	$4\frac{1}{2}$	1.9	6.67	157.3	-0.116	659.1	0.07	346.3	0.71
	$5\frac{1}{2}$	2.9	6.64	187.6	-0.139	709.8	0.06	340.5	0.73

TABLE XI—*Continued*

	$1\frac{1}{2}$	67.4	-0.041	0.04	6.66	429.8	-0.41	291.1	0.86
	$2\frac{1}{2}$	96.3	-0.054	0.04	6.66	455.8	-0.44	258.4	0.84
$\Pi_{3/2}(e)$	$3\frac{1}{2}$	125.8	-0.075	0.01	6.65	479.7	-0.44	224.2	0.88
	$4\frac{1}{2}$	155.3	-0.136	0.05	6.62	501.8	-0.43	189.0	0.98
	$5\frac{1}{2}$	179.9	0.864	4.8	-4.92	527.0	0.32	157.8	-0.78
	$\frac{1}{2}$	383.1	0.50	-	-	58.5	0.032	-	-
	$1\frac{1}{2}$	325.4	0.69	258.0	0.53	171.8	-0.010	33.1	0.12
	$2\frac{1}{2}$	291.9	0.81	195.6	0.45	260.2	-0.014	62.7	0.13
$\Sigma_{\frac{1}{2}}(e)$	$3\frac{1}{2}$	258.1	0.92	132.3	0.50	347.3	-0.020	91.9	0.16
	$4\frac{1}{2}$	223.8	1.06	68.4	0.78	433.4	-0.040	120.6	0.23
	$5\frac{1}{2}$	193.6	0.93	8.9	4.45	513.3	-0.277	144.1	0.90
	$1\frac{1}{2}$	413.5	-0.01	346.0	0.80	83.8	-0.050	54.9	0.10
	$2\frac{1}{2}$	439.7	0.10	343.4	0.82	112.4	-0.053	85.1	0.11
$\Sigma_{3/2}(e)$	$3\frac{1}{2}$	464.4	0.14	338.6	0.83	141.1	-0.053	114.4	0.13
	$4\frac{1}{2}$	487.5	0.16	332.1	0.85	169.6	-0.053	143.1	0.14
	$5\frac{1}{2}$	509.0	0.18	324.3	0.86	197.9	-0.054	171.3	0.17

a The description of the state may not be entirely accurate, see Table X

b The given state has the lower rotational quantum number.

TABLE XII

Calculated Transition Energies (cm^{-1}) and Transition Moment (10^{-30} C m) for $v = 0$ to $v = 1$ Transitions

Lower state		R BRANCH							
		Energy → $\Pi_{\frac{1}{2}}$	Moment	Energy → $\Pi_{3/2}$	Moment	Energy → $\Sigma_{\frac{1}{2}}$	Moment	Energy → $\Sigma_{3/2}$	Moment
J	$\Pi_{\frac{1}{2}}(e)$								
$\frac{1}{2}$		2941.4	0.24	3032.6	-0.057	2873.4	-0.15	2958.2	0.044
$1\frac{1}{2}$		2972.8	0.22	3086.0	-0.014	2874.1	-0.20	3001.1	0.020
$2\frac{1}{2}$		2997.2	0.22	3139.3	-0.009	2871.2	-0.20	3052.3	0.013
	$\Pi_{\frac{1}{2}}(f)$								
$\frac{1}{2}$		2941.8	0.25	3010.9	-0.041	3070.1	0.050	2893.4	-0.12
$1\frac{1}{2}$		2977.7	0.22	3058.2	0.011	3146.8	0.014	2916.6	-0.17
$2\frac{1}{2}$		3007.7	0.21	3110.5	0.009	3221.9	0.006	2939.2	-0.17
	$\Pi_{3/2}(e)$								
$1\frac{1}{2}$		2904.9	-0.016	3018.1	0.14	2806.1	-0.105	2933.2	-0.25
$2\frac{1}{2}$		2900.1	0.001	3042.2	0.14	2774.0	-0.084	2955.2	-0.25
	$\Pi_{3/2}(f)$								
$1\frac{1}{2}$		2910.3	-0.069	2990.7	0.24	3079.4	-0.061	2849.1	-0.088
$2\frac{1}{2}$		2911.4	-0.056	3014.2	0.24	3125.6	-0.049	2842.9	-0.066
	$\Sigma_{\frac{1}{2}}(e)$								
$\frac{1}{2}$		2558.0	-0.15	2649.2	-0.32	2490.1	0.66	2574.9	0.79
$1\frac{1}{2}$		2646.9	0.40	2760.1	0.12	2548.1	1.00	2675.2	-0.03
$2\frac{1}{2}$		2704.4	0.32	2846.6	0.07	2578.4	1.02	2759.5	-0.01

TABLE XII—*Continued*

	$\Sigma_{\frac{1}{2}}(f)$							
$\frac{1}{2}$	2500.2	0.011	2569.4	0.125	2628.5	0.23	2451.8	0.081
$1\frac{1}{2}$	2480.5	-0.009	2560.9	0.070	2649.6	0.25	2419.3	0.016
$2\frac{1}{2}$	2455.6	-0.005	2558.4	0.054	2669.8	0.25	2387.1	0.008
	$\Sigma_{3/2}(e)$							
$1\frac{1}{2}$	2558.9	-0.058	2672.1	0.62	2460.1	-0.041	2587.2	0.86
$2\frac{1}{2}$	2556.7	-0.102	2698.8	0.60	2430.6	-0.012	2611.7	0.87
	$\Sigma_{3/2}(f)$							
$1\frac{1}{2}$	2619.2	0.15	2699.6	0.107	2788 3	-0.028	2558.0	0.20
$2\frac{1}{2}$	2653.0	0.16	2755.8	0.084	2867.3	-0.016	2584.5	0.20
				P BRANCH				
	$\rightarrow\Pi_{\frac{1}{2}}$		$\rightarrow\Pi_{3/2}$		$\rightarrow\Sigma_{\frac{1}{2}}$		$\rightarrow\Sigma_{3/2}$	
	$\Pi_{\frac{1}{2}}(e)$							
$1\frac{1}{2}$	2847.6	0.28		-	2904.7	0.088		-
$2\frac{1}{2}$	2846.2	0.17	2937.4	0.024	2778.2	-0.27	2863.0	0.14
$3\frac{1}{2}$	2818.1	0.25	2931.3	0.014	2719.4	-0.26	2846.4	-0.12
	$\Pi_{\frac{1}{2}}(f)$							
$1\frac{1}{2}$	2857.2	0.27		-	2949.9	0.066		-
$2\frac{1}{2}$	2846.0	0.23	2915.2	0.087	2974.3	0.008	2797.6	-0.20
$3\frac{1}{2}$	2822.2	0.24	2902.7	0.055	2991.3	0.005	2761.0	-0.22

TABLE XII—*Continued*

	$\Pi_{3/2}(e)$							
$1\frac{1}{2}$	2779.6	-0.13		-	2836.7	-0.062		-
$2\frac{1}{2}$	2749.1	-0.26	2840.2	0.18	2681.1	-0.11	2765.9	0.14
$3\frac{1}{2}$	2691.0	-0.08	2804.2	0.19	2592.3	-0.10	2719.3	-0.30
	$\Pi_{3/2}(f)$							
$1\frac{1}{2}$	2789.7	-0.14		-	2882.4	-0.037		-
$2\frac{1}{2}$	2749.7	-0.17	2818.8	0.24	2878.0	-0.101	2701.3	-0.090
$3\frac{1}{2}$	2696.4	-0.14	2776.9	0.29	2865.5	-0.081	2635.2	-0.076
	$\Sigma_{\frac{1}{2}}(e)$							
$1\frac{1}{2}$	2521.6	-0.45		-	2478.7	0.67		-
$2\frac{1}{2}$	2553.4	0.24	2644.6	0.096	2485.4	0.94	2570.2	0.52
$3\frac{1}{2}$	2558.7	0.43	2671.9	0.059	2459.9	1.01	2587.0	-0.14
	$\Sigma_{3/2}(f)$							
$1\frac{1}{2}$	2359.9	-0.079		-	2452.7	0.30		-
$2\frac{1}{2}$	2293.9	-0.063	2363.0	0.092	2422.2	0.32	2245.5	-0.016
$3\frac{1}{2}$	2216.7	-0.036	2297.2	0.085	2385.8	0.34	2155.6	-0.009
	$\Sigma_{3/2}(e)$							
$1\frac{1}{2}$	2433.6	0.41		-	2490.7	-0.62		-
$2\frac{1}{2}$	2405.6	0.58	2496.8	0.67	2337.7	0.15	2422.4	-0.67
$3\frac{1}{2}$	2352.4	-0.01	2465.6	0.68	2253.7	0.08	2380.7	0.91

TABLE XII—*Continued*

	$\Sigma_{3/2}(f)$								
	$1\frac{1}{2}$	2498.6	-0.03		-	2591.3	0.091		-
	$2\frac{1}{2}$	2491.3	0.13	2560.5	0.17	2619.6	-0.017	2442.9	0.23
	$3\frac{1}{2}$	2472	0.18	2552.6	0.14	2641.3	-0.013	2411.0	0.24
					Q BRANCH				
v=0	v=1	$\Pi_{\frac{1}{2}}(e)$			$\Pi_{3/2}(e)$	$\Sigma_{\frac{1}{2}}(e)$			$\Sigma_{3/2}(e)$
	$\frac{1}{2}$	2880.3	0.25		-	2937.3	0.16		-
$\Pi_{\frac{1}{2}}(f)$	$1\frac{1}{2}$	2907.9	0.20	2999.1	0.016	2840.0	-0.15	2924.8	0.16
	$2\frac{1}{2}$	2909.7	0.27	3022.9	0.018	2811.0	-0.12	2938.0	-0.001
$\Pi_{3/2}(f)$	$1\frac{1}{2}$	2840.5	-0.143	2931.6	0.23	2772.5	-0.049	2857.3	0.11
	$2\frac{1}{2}$	2813.4	-0.027	2926.6	0.23	2714.7	-0.025	2841.7	-0.18
	$\frac{1}{2}$	2438.7	0.005		-	2495.8	0.003		-
$\Sigma_{\frac{1}{2}}(f)$	$1\frac{1}{2}$	2410.7	0.005	2501.9	-0.004	2432.7	0.0001	2427.5	-0.002
	$2\frac{1}{2}$	2357.6	0.001	2470.8	-0.004	2258.9	0.0003	2385.9	0.004
$\Sigma_{3/2}(f)$	$1\frac{1}{2}$	2549.4	-0.004	2640.5	0.018	2481.4	-0.011	2566.2	0.015
	$2\frac{1}{2}$	2555.0	0.010	2668.2	0.019	2456.3	-0.009	2583.3	-0.016
v=0	v=1	$\Pi_{\frac{1}{2}}(f)$			$\Pi_{3/2}(f)$	$\Sigma_{\frac{1}{2}}(f)$			$\Sigma_{3/2}(f)$
	$\frac{1}{2}$	2890.7	0.29		-	2983.4	0.079		-
$\pi_{\frac{1}{2}}(e)$	$1\frac{1}{2}$	2909.1	0.23	2978.3	0.064	3037.4	0.019	2860.7	-0.17
	$2\frac{1}{2}$	2916.0	0.23	2996.4	0.042	3085.1	0.009	2854.8	-0.18

TABLE XII—*Continued*

$\Pi_{3/2}(e)$	$1\frac{1}{2}$	2841.2	-0.12	2910.3	0.24	2969.5	-0.099	2792.7	-0.084
	$2\frac{1}{2}$	2818.9	-0.09	2899.3	-0.08	2988.0	-0.017	2757.7	-0.058
	$\frac{1}{2}$	2507.3	0.009		-	2600.0	0.002		-
$\Sigma_{\frac{1}{2}}(e)$	$1\frac{1}{2}$	2583.2	0.006	2652.3	0.015	2711.5	-0.004	2534.7	-0.015
	$2\frac{1}{2}$	2623.2	0.011	2703.6	0.016	2792.3	-0.003	2562.0	-0.017
$\Sigma_{3/2}(e)$	$1\frac{1}{2}$	2495.2	-0.008	2564.3	0.014	2623.4	-0.005	2446.7	-0.006
	$2\frac{1}{2}$	2475.4	-0.005	2555.9	0.016	2644.5	-0.004	2414.2	-0.005

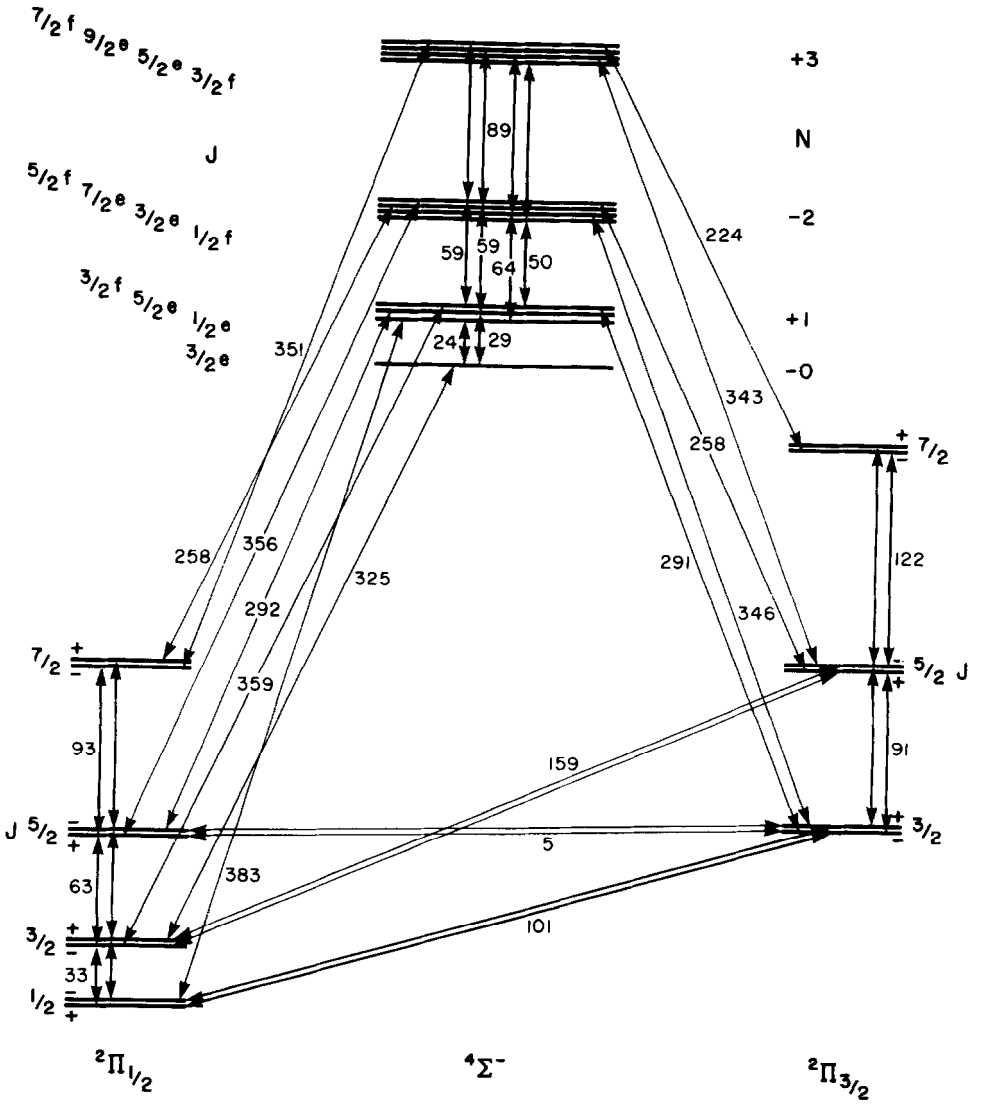

FIG. 4. Transitions between the $v = 0$ state of the $^2\Pi$ and $^4\Sigma^-$ state of NH^+. Transitions between parity doublets of the $^2\Pi$ state are also intense, but are omitted. Transition energies are in cm^{-1}.

If we turn now to transition intensities, which are proportional to the squares of matrix elements, we can compare the latter data of Table VII with the more detailed information of Tables XI and XII. As one might expect, there is good agreement between the values $\langle 0|M(x)|v\rangle$ of Table VII and the values for $^2\Pi_{1/2}$–$^2\Pi_{1/2}$, $^2\Pi_{3/2}$–$^2\Pi_{3/2}$, $^4\Sigma^-_{1/2}$–$^4\Sigma^-_{1/2}$, $^4\Sigma^-_{3/2}$–$^4\Sigma^-_{3/2}$ transitions. The analytic treatment gives no information on the transitions coupling $^2\Pi_{1/2}$ and $^2\Pi_{3/2}$ levels and so on.

The sign of C_0^v is related to the relative intensities of the P and R branches. In the

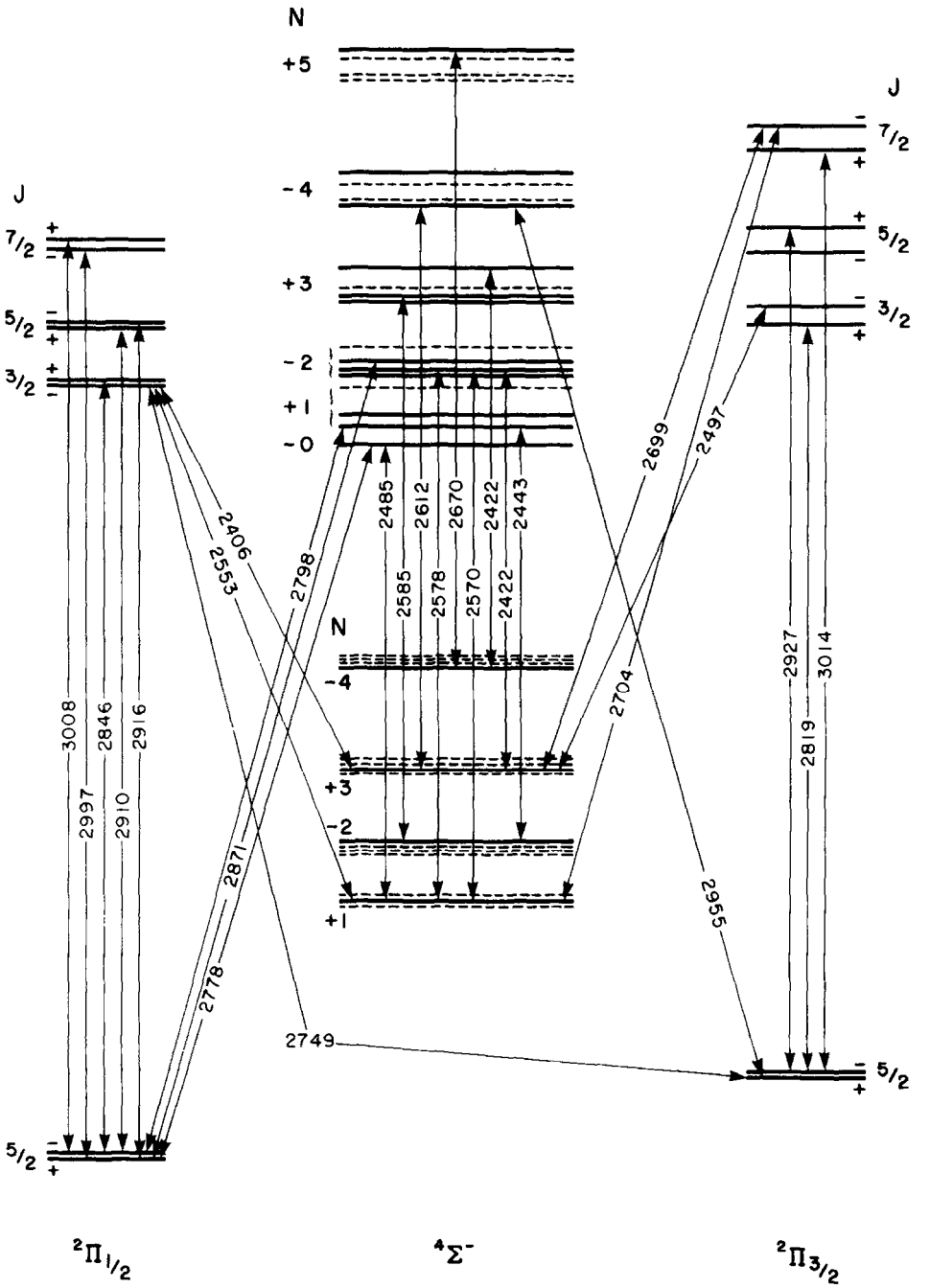

FIG. 5. Transitions from $v = 0$, $J = 2\frac{1}{2}$ states of the $^2\Pi$ and $^4\Sigma^-$ states of NH^+ to the appropriate $v = 1$ state. Dashed lines indicate $^4\Sigma^-$ states with the same N quantum number as those of interest, but with irrelevant J quantum numbers. Transition energies are in cm^{-1}.

TABLE XIII

Comparison of Calculated Potential Energy Data with Experiment

NH^+	SCF[a]	UMP3	Expt.
$V(^2\Pi)-V(^4\Sigma^-)$, $R=\infty$	2862 cm^{-1}	6808 cm^{-1}	7666 cm^{-1} [b]
$V(^2\Pi)-V(^4\Sigma^-)$, $R=R_e$	3021 cm^{-1}	1630 cm^{-1}	-550 cm^{-1} [c]
$V(\infty)-V(R_e)$, $^2\Pi$	31176 cm^{-1}	34522 cm^{-1}	
$V(\infty)-V(R_e)$, $^4\Sigma^-$	31335 cm^{-1}	29344 cm^{-1}	
R_e $^2\Pi$	1.087×10^{-10} m	1.068×10^{-10} m	1.070×10^{-10} m [c]
R_e $^4\Sigma^-$	1.070×10^{-10} m	1.090×10^{-10} m	
CH			
$V(^2\Pi)-V(^4\Sigma^-)$, $R=\infty$		0	
$V(^2\Pi)-V(^4\Sigma^-)$, $R=R_e$		-4370 cm^{-1} [d]	-5844 cm^{-1} [e]

a Three configuration wavefunction for $X^2\Pi$ state, one configuration for $a^4\Sigma^-$ state.

b Derived from data in C.E. Moore, Atomic Energy Levels, National Bureau of Standards (1949).

c Ref. 3.

d Using experimental R_e. $V(^2\Pi, 1.120\times10^{-10}$ m) = -38.395285 hartree, $V(^4\Sigma^-, 1.085\times10^{-10}$ m) = -38.375375 hartree.

e A. Kasdan, E. Herbst and W.C. Lineberger, Chem. Phys. Lett. 31, 78-80 (1975).

present case we have C_0^1 negative, so indicating a relatively strong P branch. In general the detailed results of Tables XI and XII are in accord with this. A significant exception occurs with transitions between $^4\Sigma^-$ e-type levels. This is presumably due to variations in the degree of mixing of $^2\Pi$ and $^4\Sigma^-$ configurations, but the interaction is so complicated that it is difficult to state more than that.

The effects of the perturbations may be clearly seen in the $v = 1$ levels shown in

TABLE XIV

Configuration Weights in the MCSCF Wavefunction and Spin Expectation Value for the UHF Wavefunction Describing the $X^2\Pi$ State of NH^+

Internuclear distance /10^{-10} m	Weights			$\langle S^2 \rangle$
	$3\sigma^2$	$4\sigma^2$	$3\sigma 4\sigma$	
1.1	0.9929	-0.1096	0.0460	0.757
1.2	0.9901	-0.1291	0.0549	0.759
1.3	0.9865	-0.1502	0.0655	0.764
1.4				0.782
1.5	0.9760	-0.1970	0.0931	0.850
1.6				1.002
1.7	0.9599	-0.2478	0.1315	1.163

Fig. 5. First, the ordering of the $^2\Pi_{3/2}$ parity doublets is reversed, and the separation between them increased. Second, the energies of the $^4\Sigma^-$ states differ substantially from the pattern expected for a Hund's case (b) system. In contrast, Fig. 4 shows that the $v = 0$ levels are well behaved.

A somewhat unexpected prediction is that the transitions from the $^2\Pi_{1/2}$ ($v = 0$) to $^2\Pi_{3/2}$ ($v = 0$) are fairly intense. Analogous transitions observed in the case of nitrogen(II) oxide (*27*) were relatively weak, and were thought to be magnetic dipole transitions. The corresponding vibrational transitions are also predicted to be more intense than is found for nitrogen(II) oxide (*28*). However, it is clear that the most intense of the "forbidden" transitions are from $^2\Pi$ to $^4\Sigma^-$ states, rather than between the different $^2\Pi$ components.

CONCLUSIONS

The present study is one of the first attempts to make a quantitative prediction of vibrational–rotational spectra involving strongly interacting states. We predict that the spectrum of NH^+ should be complicated, with relatively strong $^2\Pi_{1/2}$–$^2\Pi_{3/2}$ transitions and $^2\Pi$–$^4\Sigma^-$ transitions. As a by-product of our investigation we have been able to suggest assignments of previous unidentified spectral lines.

We hope that our results will aid identification of NH^+ in atmospheric or astrophysical sources through observation of its infrared spectrum.

RECEIVED: March 21, 1983

REFERENCES

1. M. W. FEAST, *Astrophys. J.* **114,** 344–355 (1951).
2. G. KRISHNAMURTHY AND M. SARASWATHY, *Pramana* **6,** 235–243 (1976).
3. R. COLIN AND A. E. DOUGLAS, *Canad. J. Phys.* **46,** 61–73 (1968).
4. I. D. L. WILSON, *Mol. Phys.* **36,** 597–610 (1978).
5. H. P. D. LIU AND G. VERHAEGEN, *J. Chem. Phys.* **53,** 735–745 (1970).
6. P. ROSMUS AND W. MEYER, *J. Chem. Phys.* **66,** 13–19 (1977).
7. M. F. GUEST AND D. M. HIRST, *Mol. Phys.* **34,** 1611–1621 (1977).
8. K. RUEDENBERG, L. M. CHEUNG, AND S. T. ELBERT, *Int. J. Quantum Chem.* **16,** 1069–1101 (1979).
9. C. MØLLER AND M. S. PLESSET, *Phys. Rev.* **46,** 618–622 (1934).
10. J. A. POPLE, J. S. BINKLEY, AND R. SEEGER, *Int. J. Quantum Chem. Symp.* **10,** 1–20 (1976).
11. J. A. POPLE AND R. K. NESBET, *J. Chem. Phys.* **22,** 571–572 (1954).
12. L. FARNELL AND R. H. NOBES, unpublished.
13. J. A. POPLE *et al., QCPE* **13,** 406 (1981).
14. J. F. OGILVIE, W. R. RODWELL, AND R. H. TIPPING, *J. Chem. Phys.* **73,** 5221–5229 (1980).
15. S. HUZINAGA, *J. Chem. Phys.* **42,** 1293–1302 (1965).
16. S. HUZINAGA, "Approximate Atomic Wavefunctions," University of Alberta, Edmonton, 1971.
17. F. B. VAN DUIJNEVELDT, IBM (unpublished).
18. J. M. HUTSON, *J. Phys. B* **14,** 851–857 (1981).
19. J. M. HUTSON, *QCPE Bull.* **2,** 435 (1982).
20. J. F. OGILVIE, *Proc. R. Soc. London Ser. A,* **378,** 287–300 (1981); erratum **381,** 479 (1982).
21. J. F. OGILVIE AND M. H. A. HASAN, *J. Mol. Struct.* **75,** 255–264 (1981).
22. R. H. TIPPING AND J. F. OGILVIE, *J. Mol. Struct.* **35,** 1–55 (1976).
23. R. H. TIPPING AND J. F. OGILVIE, *Int. Rev. Phys. Chem.,* in press.
24. R. H. TIPPING AND J. F. OGILVIE, *J. Mol. Spectrosc.* **96,** 442–450 (1982).
25. P. C. ENGELKING, R. R. CORDERMANN, J. J. WENDOLOSKI, G. B. ELLISON, S. V. O'NEILL, AND W. C. LINEBERGER, *J. Chem. Phys.* **74,** 5460–5473 (1981) and references therein.
26. D. FELLER, L. E. MCMURCHIE, W. T. BORDEN, AND E. R. DAVIDSON, *J. Chem. Phys.* **77,** 6134–6143 (1982).
27. J. M. BROWN, A. R. H. COLE, AND F. R. HONEY, *Mol. Phys.* **23,** 287–295 (1972).
28. T. C. JAMES, *J. Chem. Phys.* **40,** 762–771 (1964).